An extended shoving model for dynamic fluctuation of glass transition in amorphous polymer towards cooperative shape-memory effect

Jingyun Liu[1], Haibao Lu[1,3], Ahmed Elmarakbi[2] and Yong-Qing Fu[2,3]

[1]National Key Laboratory of Science and Technology on Advanced Composites in Special Environments, Harbin Institute of Technology, Harbin 150080, P.R. China

[2]Faculty of Engineering and Environment, Northumbria University, Newcastle upon Tyne NE1 8ST, UK

[3]E-mail: luhb@hit.edu.cn and richard.fu@northumbria.ac.uk

Abstract: Phase transition theory is a powerful approach to study shape-memory effect (SME) and dynamic relaxation behavior in amorphous shape-memory polymers (SMPs) undergoing glass transition processes. However, previous studies are mostly limited to building-up of experimental models, mainly due to poor understanding of dynamic fluctuation of glass transition. In this study, the dynamic fluctuation of glass transition in the amorphous SMPs, whose thermodynamic SME is governed by the phase transition theory, was investigated using a shoving model. A constitutive relationship between potential energy and cooperatively rearranging region (CRR) volume is firstly developed to explore the working principle of phase transition in the thermodynamic SME of amorphous SMPs, based on the shoving model and Adam-Gibbs domain size model. Effect of CRR volume on the phase transition is further formulated using the strain function, and then employed to develop a constitutive stress-strain equation based on the extended Maxwell model. The working principles of cooperative SME and dynamic relaxation behaviors have been explored and

discussed. Finally, effectiveness of the analytical results obtained using the proposed model has been verified using the experimental results of amorphous SMPs reported in literature.

Keywords: shape memory polymer; amorphous; cooperative; dynamic fluctuation

1. Introduction

Stimulus-responsive polymers, which have capabilities of responding to the environmental stimulations [1-7], have attracted great attention in the scientific community. Due to their numerous advantages, including designable properties [8-10], excellent biodegradability and biocompatibility [11], these stimulus-responsive polymers have shown great potential applications in biomedical devices [12-14], flexible electronics [15,16], smart robotics [17] and space deployable structures [18,19]. Among them, stimulus-responsive shape memory polymers (SMPs) have been extensively studied due to their tailorable dynamics with shape memory effect (SME) and shape recovery behavior [20,21].

For the SMPs, the stored strain energy has been identified as the driving force to determine the dynamic glass transition and SME in amorphous SMPs with various and tailorable relaxation behaviors [22,23]. To understand the working principles of glass transition in amorphous SMPs, considerable effort has been made to develop various constitutive models in the past three decades. For example, Nguyen *et al*. [24] established a thermoviscoelastic model to describe the structural relaxation and viscous flow based on the Adam-Gibbs model and Eyring equation. Liu *et al* [25] developed a phase transition model for the frozen phase transition and characterize the

release of stored strain energy in the amorphous SMP undergoing glass transitions. Li *et al*. [26,27] proposed an extended phase transition model to describe the effect of strain rate on the dynamic phase transition of amorphous SMPs. Wang *et al.* [28] developed a phenomenological model to describe the tailorable shape transition behavior of SMPs undergoing dynamically multiple phase transitions. These studies are well able to reflect the constitutive relationship between dynamic glass transition and SME. However, the working principle of thermodynamic fluctuation in the phase transition of amorphous SMP has not been well understood, thus so far it is still impossible to formulate a dynamic equilibrium for the glass transition for the SMPs. Currently most studies are still at the phenomenological and experiential model building stages for explaining the glass transitions and its thermodynamic fluctuation.

Based on the phase transition theory [25] and shoving model [29], this study is focused on clarifying the working principles of glass transition in the amorphous SMP using the functions of potential energy and average number of dynamic segments in cooperatively rearranging region (CRR) [30]. A constitutive relationship of potential energy and CRR volume is initially established to quantitatively describe the effect of shear modulus on thermodynamic SME of the amorphous SMP, according to the Adam-Gibbs domain size model [31]. Effect of CRR volume on the phase transition has been formulated using the strain function, which has been further employed to develop a constitutive stress-strain equation based on the extended Maxwell model [32]. Finally, effectiveness of analytical result of proposed model has been verified

using the experimental results reported in the literature [33-36], and good agreements between these analytical and experimental results of amorphous SMPs are achieved.

2. Theoretical framework

According to the Adam-Gibbs domain size model [31], there are a large number of dynamic segments in polymer chains, which can form various CRRs in response to the external stimulus fields [29,37]. At a low ambient temperature, if the mutual attraction forces among the segments are larger than those of the repulsion ones, the CRRs will be stacked closely. With an increase in the temperature, the repulsion force is increased, causing the rearrangement and dynamic relaxation of the CRRs, as well as the changes of CRR volumes of amorphous polymers, as shown in Figure 1(a).

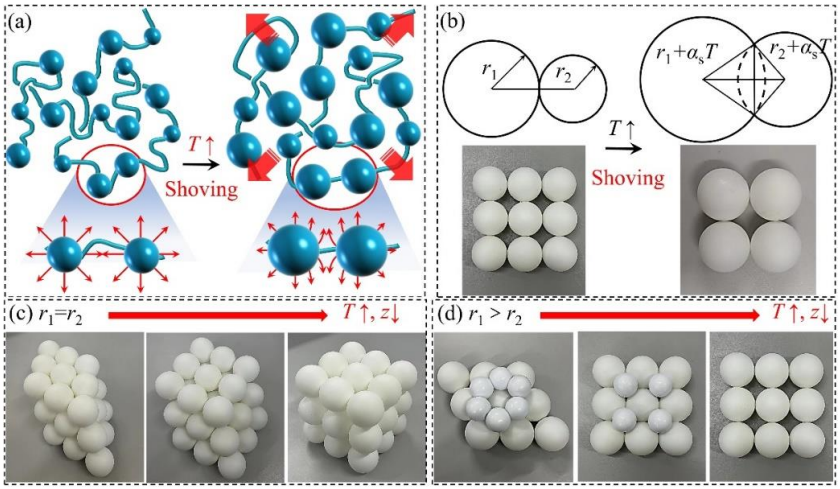

Figure 1. Schematic illustrations of the shoving model for the CRR filled with dynamic segments. (a) Segment rearrangement. (b) Geometric topology. (c) Effect of temperature on the average number of dynamic segments in CRR with $r_1=r_2$. (d) Effect of temperature on the average number of dynamic segments in CRR with $r_1>r_2$, where r_1 and r_2 are the radii of the CRRs.

Meanwhile, transition of geometric topology is triggered and the average number of dynamic segments in the CRR is increased, as shown in Figure 1(b). Figures 1(c) and 1(d) illustrate the effects of temperature on the geometric topology and average

number of dynamic segments in the characteristic CRRs.

According to the shoving model [29], the temperature dependent relaxation time ($\tau(T)$) of a CRR can be written as,

$$\tau(T) = \tau_0 \exp\left[\frac{\Delta F(T)}{k_B T}\right] \tag{1}$$

where τ_0 is the perfector of relaxation time, $\Delta F(T)$ is the free energy barrier [29], k_B=1.38×10^{-23} J//K is the Boltzmann's constant, and T is the temperature.

The free energy barrier ($\Delta F(T)$) is proportional to the instantaneous (infinite-frequency) shear modulus ($G_\infty(T)$) [29],

$$\Delta F(T) = G_\infty(T) V_c \tag{2}$$

where V_c is the characteristic volume of CRR [29].

This instantaneous shear modulus ($G_\infty(T)$) has a constitutive relationship with the temperature (T) for the CRR, which can be expressed as [38],

$$\log\frac{G_\infty(T)}{G_0} = \log\frac{G(T^{ref})}{G_0} - \alpha(T - T^{ref}) \tag{3}$$

where G_0 is the initial shear modulus, $G(T^{ref})$ is the shear modulus at the reference temperature (T^{ref}), and α is the thermal expansion coefficient of the CRR.

The characteristic volume (V_c) of CRR can be written as [29],

$$V_c = \frac{2}{3}\frac{(\Delta V)^2}{V} \tag{4}$$

where ΔV is the activation volume during shoving, and V is the characteristic volume of CRR before shoving and rearrangement.

According to the shoving model [29], the CRR can be regarded as a cooperatively rearrangement of spheres, of which the change in volume (V_s) of a CRR can be

expressed as,

$$V_s = \int_{r_1+\alpha_s\left(\frac{r_1-r_2}{r_1+r_2}\right)\left(T-T^{\mathrm{ref}}\right)}^{r_1+\alpha_s\left(T-T^{\mathrm{ref}}\right)} \pi\left\{\left[r_1+\alpha_s\left(T-T^{\mathrm{ref}}\right)\right]^2 - x^2\right\}\mathrm{d}x$$

$$= \pi\left\{\left[r_1+\alpha_s\left(T-T^{\mathrm{ref}}\right)\right]^2 x - \frac{x^3}{3}\right\}\Bigg|_{r_1+\alpha_s\left(\frac{r_1-r_2}{r_1+r_2}\right)\left(T-T^{\mathrm{ref}}\right)}^{r_1+\alpha_s\left(T-T^{\mathrm{ref}}\right)} \tag{5}$$

$$= \frac{\pi}{3}\left\{\left[r_1+\alpha_s\left(T-T^{\mathrm{ref}}\right)\right]^2\left[\alpha_s\left(\frac{\frac{5r_2}{r_1}-1}{1+\frac{r_2}{r_1}}\right)\left(T-T^{\mathrm{ref}}\right)-r_1\right]+\left[r_1+\alpha_s\frac{1-\frac{r_2}{r_1}}{1+\frac{r_2}{r_1}}\left(T-T^{\mathrm{ref}}\right)\right]^3\right\}$$

where r_1 and r_2 are the radii of the CRR, α_s is the thermal expansion coefficient of the spherical CRR.

The change in volume (ΔV) of total CRRs can be obtained as follows [29],

$$\Delta V = \frac{4\pi\left[r_1+\alpha_s\left(T-T^{\mathrm{ref}}\right)\right]^3}{3} - \frac{4\pi r_1^3}{3} - zV_s \tag{6}$$

where z is average number of dynamic segments in the CRR.

Based on the Adam-Gibbs domain size model [31,39], the average number (z) of dynamic segments in the CRR is determined by the temperature (T),

$$z = \frac{T^* - T_0}{T^*}\frac{T}{T-T_0} \tag{7}$$

where T^* is the specific temperature, at which each CRR can relax independently, T_0 is the specific temperature, at which all the CRRs are involved into a domain and relaxed cooperatively.

Combining equations (1), (2), (3), (4), (6) and (7), the relaxation time ($\tau(T)$) and the change in volume (ΔV) of the total CRRs can be obtained as,

$$\tau(T)=\tau_0\exp\left[\frac{2\left(\Delta V\right)^2 G(T^{\mathrm{ref}})10^{-\alpha(T-T^{\mathrm{ref}})}}{3k_{\mathrm{B}}TV}\right] \tag{8a}$$

$$\Delta V=\frac{4\pi\left[r_1+\alpha_{\mathrm{s}}\left(T-T^{\mathrm{ref}}\right)\right]^3}{3}-\frac{4\pi r_1^3}{3}-\frac{T^*-T_0}{T^*}\frac{T}{T-T_0}V_{\mathrm{s}} \tag{8b}$$

Based on the phase transition theory [25], the phase evolution function (ϕ_{f}) is determined by the stored strain (ε_{s}) and pre-stored strain ($\varepsilon_{\mathrm{pre}}$) as,

$$\phi_{\mathrm{f}}=\frac{\varepsilon_{\mathrm{s}}}{\varepsilon_{\mathrm{pre}}}=1-A\exp\left[-\frac{2\left(\Delta V\right)^2 G(T^{\mathrm{ref}})10^{-\alpha(T-T^{\mathrm{ref}})}}{3k_{\mathrm{B}}TV}\right] \tag{9}$$

where A is the material constant.

Combining equations (5), (8) and (9), the total strain (ε) can be obtained as,

$$\varepsilon=\varepsilon_0+\varepsilon_s=\varepsilon_0+\varepsilon_{\mathrm{pre}}\phi_{\mathrm{f}}=\varepsilon_0+\varepsilon_{\mathrm{pre}}\left\{1-A\exp\left[-\frac{2\left(\Delta V\right)^2 G(T^{\mathrm{ref}})10^{-\alpha(T-T^{\mathrm{ref}})}}{3k_{\mathrm{B}}TV}\right]\right\} \tag{10a}$$

$$\begin{aligned}\Delta V=&\frac{4\pi\left\{\left[r_1+\alpha_{\mathrm{s}}\left(T-T^{\mathrm{ref}}\right)\right]^3-r_1^3\right\}}{3}-\frac{T^*-T_0}{T^*}\frac{T}{T-T_0}\frac{\pi}{3}\cdot\\&\left\{\left[r_1+\alpha_{\mathrm{s}}\left(T-T^{\mathrm{ref}}\right)\right]^2\left[\alpha_{\mathrm{s}}\left(\frac{\frac{5r_2}{r_1}-1}{1+\frac{r_2}{r_1}}\right)\left(T-T^{\mathrm{ref}}\right)-r_1\right]+\left[r_1+\alpha_{\mathrm{s}}\frac{1-\frac{r_2}{r_1}}{1+\frac{r_2}{r_1}}\left(T-T^{\mathrm{ref}}\right)\right]^3\right\}\end{aligned} \tag{10b}$$

where ε_0 is the initial strain.

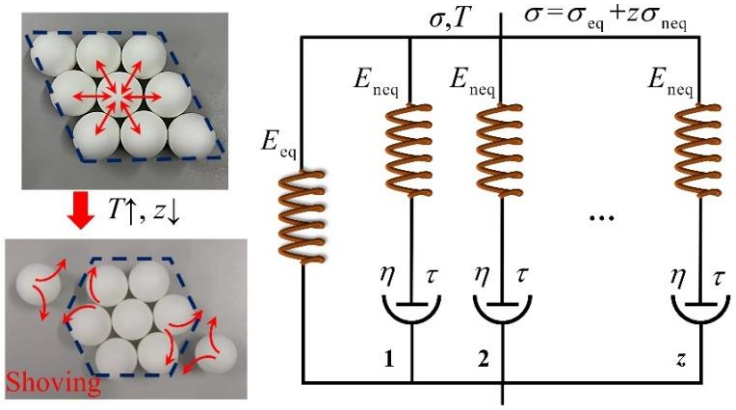

Figure 2. Schematic illustrations of average number of dynamic segments in CRR and rheological behavior of the CRR using the extended Maxwell model.

Figure 2 illustrates the effects of average number of dynamic segments in the CRR

on rheological behaviors of the CRR (in which there are z dynamic segments) and on average number of dynamic segments in the CRR [30]. Based on the extended Maxwell model, the thermodynamic behaviors of these dynamic segments can be further characterized using the non-equilibrium branches of the CRR.

Based on the Maxwell model, the constitutive stress-strain relationship of CRR can be expressed as [32],

$$\sigma = \sigma_{eq} + \sum^{z} \sigma_{neq} = \sigma_{eq} + z\sigma_{neq}, \quad \varepsilon = \varepsilon_{eq} = \varepsilon_{neq} \tag{11a}$$

$$\varepsilon = \frac{\sigma_{eq}}{E_{eq}} \tag{11b}$$

$$\frac{d\varepsilon}{dt} = \frac{1}{E_{neq}} \frac{d\sigma_{neq}}{dt} + \frac{\sigma_{neq}}{\eta} \tag{11c}$$

where σ and ε are the stress and strain of the CRR, respectively. σ_{eq} and ε_{eq} are the stress and strain of the equilibrium branch, respectively. σ_{neq} and ε_{neq} are the stress and strain of the non-equilibrium branch, respectively. E_{eq} and E_{neq} are the moduli of the equilibrium branch and non-equilibrium branch, respectively. Finally, η is the viscosity of the non-equilibrium branch.

Based on equation (11), the storage modulus (E') can be further obtained as [32],

$$E' = E_{eq} + \sum^{z} E_{neq} \frac{\omega^2\tau^2}{1+\omega^2\tau^2} = E_{eq} + E_{neq} \frac{T^* - T_0}{T^*} \frac{T}{T - T_0} \frac{\omega^2\tau^2}{1+\omega^2\tau^2} \tag{12}$$

where ω is the frequency.

The constitutive stress-time relationship of the CRR can be obtained accordingly,

$$\sigma(t) = \sigma_{eq} + \sigma_{neq} = \varepsilon_0 E_{eq} + \left(\sigma_0 - \varepsilon_0 E_{eq}\right) \exp(-\frac{t}{\tau}), \left(\tau = \frac{\eta}{E_{neq}} \right) \tag{13}$$

where ε_0 is the given constant strain, σ_0 is the initial stress (at t=0 s).

Finally, by combining equations of (10a), (12) and (13), the constitutive stress-strain, storage modulus-temperature and strain-temperature relationships can be obtained.

$$\begin{cases} \sigma(t)=\sigma_{eq}+\sigma_{neq}=\varepsilon_0 E_{eq}+\left(\sigma_0-\varepsilon_0 E_{eq}\right)\exp(-\frac{t}{\tau}),\left(\tau=\frac{\eta}{E_{neq}}\right) \\ E^{'}=E_{eq}+\sum^{z}E_{neq}\frac{\omega^2\tau^2}{1+\omega^2\tau^2}=E_{eq}+E_{neq}\frac{T^*-T_0}{T^*}\frac{T}{T-T_0}\frac{\omega^2\tau^2}{1+\omega^2\tau^2} \\ \varepsilon=\varepsilon_0+\varepsilon_s=\varepsilon_0+\varepsilon_{pre}\phi_f=\varepsilon_0+\varepsilon_{pre}\left\{1-A\exp\left[-\frac{2(\Delta V)^2 G(T^{ref})10^{-\alpha(T-T^{ref})}}{3k_B TV}\right]\right\} \end{cases} \quad (14)$$

To verify the effectiveness of the equation (10), analytical results of strain-temperature curves were obtained with the different size ratios (r_2/r_1) and thermal expansion coefficients (α_s) of the CRRs, and are shown in Figure 3. The values of parameters used in equation (10) for the calculations are ε_0=0%, ε_{pre}=10% [34], A=1, r_1=1×10^{-9} m, T^{ref}=270 K, T^*=750 K, T_0=275 K, G=3 GPa, α=0.031 K^{-1} [32,40]. As shown in Figure 3(a), with an increase in the size ratio (r_2/r_1) of the CRR from 0.2, 0.4, 0.6, 0.8 to 1.0, the shape recovery temperature is decreased from 395 K, 392 K, 389 K, 386 K to 384 K, at the given recovery strain of ε=1% and thermal expansion coefficient of α_s=3×10^{-12} m/K.

Meanwhile, Figure 3(b) shows that when the shape recovery temperature is increased from 371 K, 392 K, 402 K, 410 K, 415 K with an increase in the thermal expansion coefficient (α_s) of the CRR from 1×10^{-12} m/K, 3×10^{-12} m/K, 5×10^{-12} m/K, 7×10^{-12} m/K to 9×10^{-12} m/K, at the given recovery strain of ε=1% and size ratio of r_2/r_1=0.4. These analytical results indicate that the size ratio (r_2/r_1) and thermal expansion coefficient (α_s), which quantifies the shoving and repulsion forces among

the CRRs, respectively, play essential roles to influence their thermodynamic behaviors.

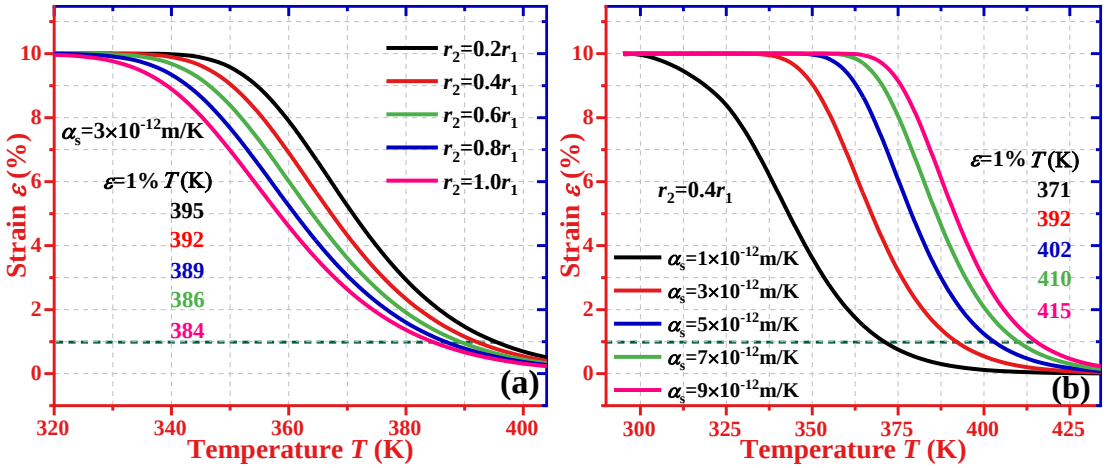

Figure 3. The strain-temperature curves calculated using the proposed model of equation (10). (a) For the effect of size ratio (r_2/r_1) on the thermodynamic behavior. (b) For the effect of thermal expansion coefficient on the thermodynamic behavior.

Effects of size ratio (r_2/r_1) of CRR and the thermal expansion coefficient (α_s) on the storage modulus-temperature of the CRRs were further investigated based on equation (12), and the obtained results are plotted in Figure 4. The values of parameters used in equation (12) for the calculations are E_{eq}=5 MPa, E_{neq}=2000 MPa [35], τ_0=0.01 s, r_1=1×10^{-9} m, T^{ref}=290 K, T^*=750 K, T_0=265 K, G=3 GPa, α=0.04 K^{-1}, ω=8 s^{-1}[32,40].

Figure 4(a) shows that with an increase in the size ratio (r_2/r_1) from 0.2, 0.4, 0.6, 0.8 to 1.0, the shape recovery temperature is decreased from 384 K, 382 K, 379 K, 376 K to 374 K at the same storage modulus of E'=50 MPa and thermal expansion coefficient of α_s=3×10^{-12} m/K. As shown in Figure 4(b), the shape recovery temperature is increased from 375 K, 386 K, 396 K, 402 K, 407 K, with an increase in the thermal expansion coefficient (α_s) from 1×10^{-12} m/K, 3×10^{-12} m/K, 5×10^{-12} m/K, 7×10^{-12} m/K to 9×10^{-12} m/K, at the same storage modulus of E'=40 MPa and size ratio

of r_2/r_1=0.4. These analytical results indicate that the size ratio (r_2/r_1) and thermal expansion coefficient (α_s) play essential roles to determine the thermomechanical modulus of the CRR [22,40].

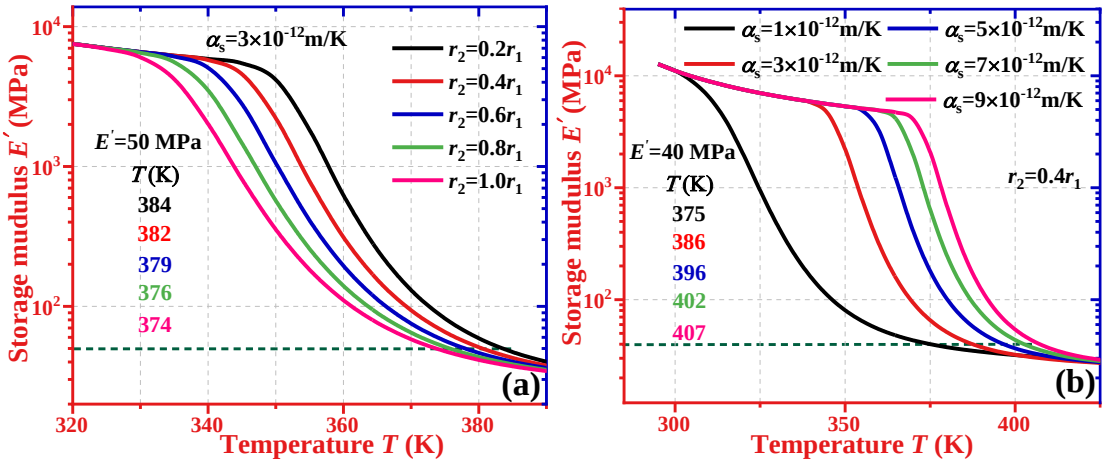

Figure 4. The storage modulus-temperature curves calculated using the proposed model (12). (a) For the effect of size ratio (r_2/r_1) on the thermodynamic behavior. (b) For the effect of thermal expansion coefficient on the thermodynamic behavior.

Furthermore, effects of size ratio (r_2/r_1) and the thermal expansion coefficient (α_s) on the constitutive stress-time relationship of the CRRs were investigated based on equation (14), and the obtained results are plotted in Figure 5. The values of parameters used in equation (14) for the calculations are $\varepsilon_0 E_{eq}/\sigma_0$=0.1 [36], τ_0=0.1 s, r_1=1×10^{-9} m, T^{ref}=300 K, T^*=750 K, T_0=330 K, G=3 GPa, α=0.049 K^{-1} [32,40].

Figure 5(a) shows that the relaxation time is decreased from 54 s, 34 s, 22 s, 15 s to 12 s, with an increase in the size ratio (r_2/r_1) from 0.4, 0.41, 0.42, 0.43 to 0.44, at the same thermal expansion coefficient of α_s=8.5×10^{-12} m/K. Meanwhile, as the results shown in Figure 5(b), the relaxation time is increased from 9 s, 12 s, 19 s, 31 s to 54 s, with an increase in the thermal expansion coefficient (α_s) from 8.1×10^{-12} m/K, 8.2×10^{-12} m/K, 8.3×10^{-12} m/K, 8.4×10^{-12} m/K to 8.5×10^{-12} m/K, at the same size ratio of

r_2/r_1=0.4. These results reveal that the constitutive stress-time relationship is mainly determined by the size ratio (r_2/r_1) and thermal expansion coefficient (α_s) of the CRR.

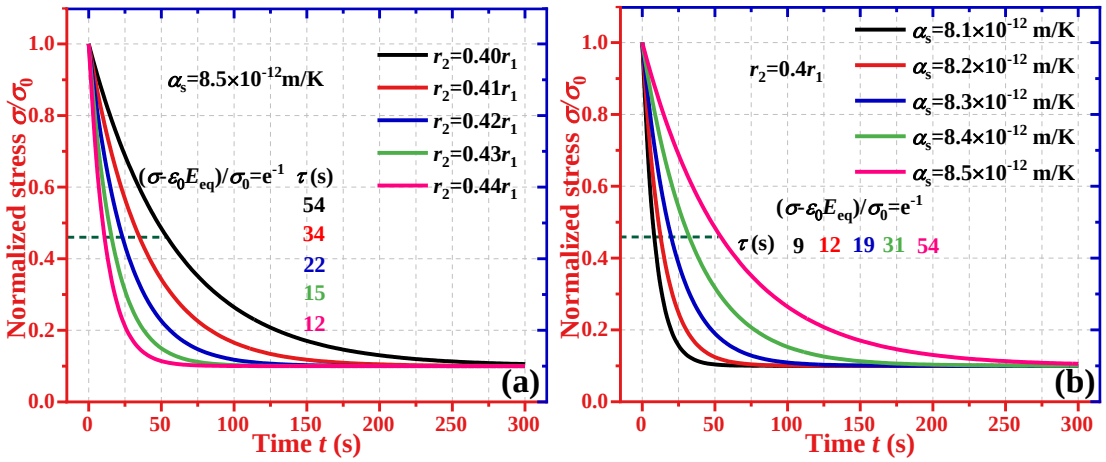

Figure 5. The normalized stress-relaxation curves calculated using the proposed model (14). (a) For the effect of size ratio (r_2/r_1) on the thermodynamic behavior. (b) For the effect of thermal expansion coefficient on the thermodynamic behavior.

3. Experimental verification

To verify the effectiveness of the proposed model based on the equation (10), the experimental data of strain-temperature behaviors of epoxy SMP [33] were used, and the corresponding analytical results obtained using equation (10) are plotted in Figure 6(a). All the parameters used in the calculation based on equation (10) are listed in Table 1, where A=1, r_1=1×10^{-9} m, T^{ref}=300 K, T^*=750 K, T_0=375 K, G=3 GPa [32,40].

Table 1. Values of parameters used in equation (10) for epoxy SMP [33].

Average lateral distance (Å)	ΔV(m^3)	r_2/r_1	α_s (m/K)	α(K^{-1})
3.78	4.79×10^{-29}	0.74	2.96×10^{-11}	0.040
4.10	5.61×10^{-29}	0.98	1.58×10^{-11}	0.031
4.32	6.21×10^{-29}	1.01	1.44×10^{-11}	0.029
4.35	6.29×10^{-29}	1.18	1.18×10^{-11}	0.026

As shown in Figure 6(a), the stored strain of CRR is decreased from 6.5%, 4.5%, 2.9% to 2.2% with the average lateral distance between the neighboring chains in the

CRR increased from 3.78 Å, 4.10 Å, 4.32 Å to 4.35 Å. It reveals that with the increment of the average lateral distance, the value of r_2/r_1 increases, leading to the decreased activation volume (ΔV) of the total CRRs and also the decreased stored strains (ε_s). Figure 6(b) shows the correlation index R^2 between the analytical and experimental results [33], which are 99.14%, 98.67%, 98.48% and 98.62% for the cases of average lateral distances of 3.78 Å, 4.10 Å, 4.32 Å and 4.35 Å, respectively.

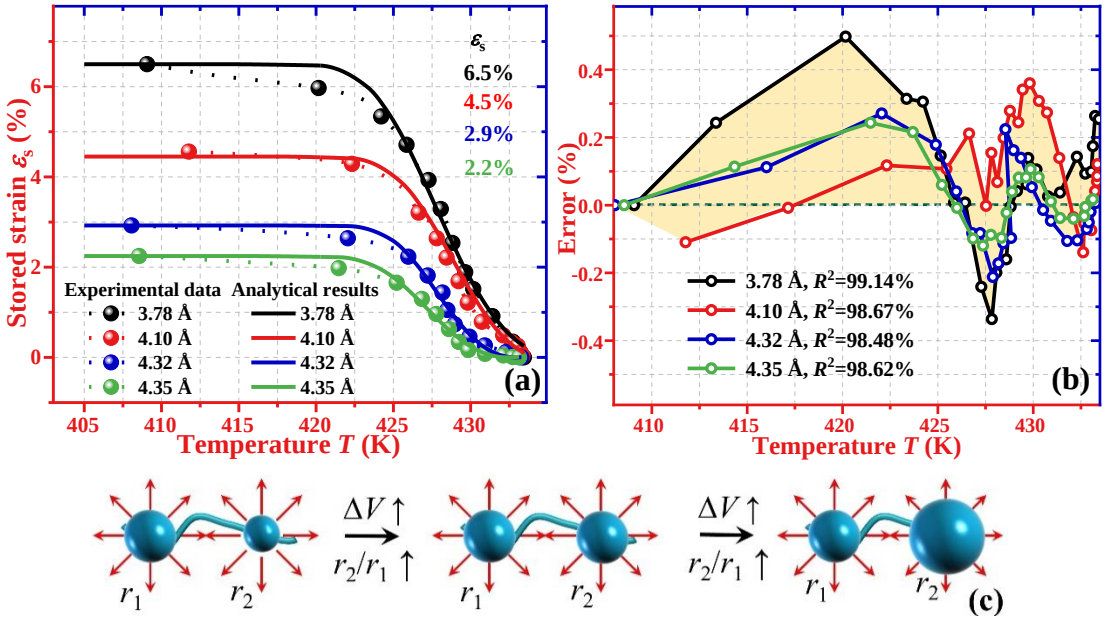

Figure 6. Comparisons of analytical results using equation (10) and experimental data [33] of the stored strain as a function of temperature for epoxy SMP. (a) The stored strain-temperature curves. (b) Divergences of analytical and experimental results of stored strain. (c) Schematic illustration of the repulsion force with various radius ratio (r_2/r_1) of CRRs.

Figure 6(c) shows the working principle for the effects of average lateral distance for the CRR. During the shoving process among the CRRs, the activation volume (ΔV) of the total CRRs is increased with an increase in the radius ratio (r_2/r_1), which is mainly resulted from the increase in the average lateral distance. The repulsion force has been identified as the driving force [29], and the average lateral distance of the CRR is gradually enlarged with an increase in the repulsion force during the shoving

process. Therefore, the radius ratio (r_2/r_1) and activation volume (ΔV) of total CRRs are then increased, resulting in the decreased repulsion force until a new dynamic equilibrium of stored strain is reached.

To further verify the equation (10), the experimental data of strain-temperature behavior of DETDA-D230 (DETDA: Diethyltoluenediamine; D230: poly(propylene glycol) bis (2-aminopropyl) ether) SMPs with various molar ratios of DETDA of 0% and 60% were applied [34]. The analytical results calculated based on the equation (10) were obtained and they are plotted in Figure 7. All the parameters used in the calculations based on equation (10) are listed in Table 2, where A=1, r_1=1×10^{-9} m, T^{ref}=300 K, T^*=750 K, T_0=320K, G=3 GPa [32,40]. With an increase in the molar ratio of DETDA from 0% to 60%, the stored strain has been completely released at the temperatures of 380 K and 405 K, respectively, but at the same total strain of ε=1.80%, as shown in Figure 7(a). Figure 7(b) shows the correlation index R^2 between the analytical and experimental results [34], which are 98.05% and 98.15% for the DETDA molar ratio of 0% and 60%, respectively. The analytical results obtained using equation (10) agree well with the experimental data ($|\Delta\varepsilon|$<0.9%).

Table 2. Values of parameters used in equation (10) for DETDA-D230 SMP [34].

Samples	r_2/r_1	α_s (m/K)	α(K^{-1})
0% DETDA	19.00	1.26×10^{-10}	0.150
60% DETDA	2.40	1.12×10^{-11}	0.024

Figure 7(c) shows the effect of radius ratio (r_2/r_1) on the shape recovery behaviour of the DETDA SMPs. The radius ratio (r_2/r_1) of CRRs is increased with an increase in the increase in the molar ratio of DETDA. The working principle of molar ratio of

DETDA in the SMP is also originated from the effect of radius ratio (r_2/r_1) on the activation volume (ΔV) of total CRRs. The repulsion force has been identified as the driving force [29], and the radius ratio (r_2/r_1) is gradually increased with an increase in the repulsion force during the shoving process of the CRR. Therefore, the activation volume (ΔV) is increased accordingly, resulting in the decreased repulsion forces until a new dynamic equilibrium of shape recovery strain relaxation is reached.

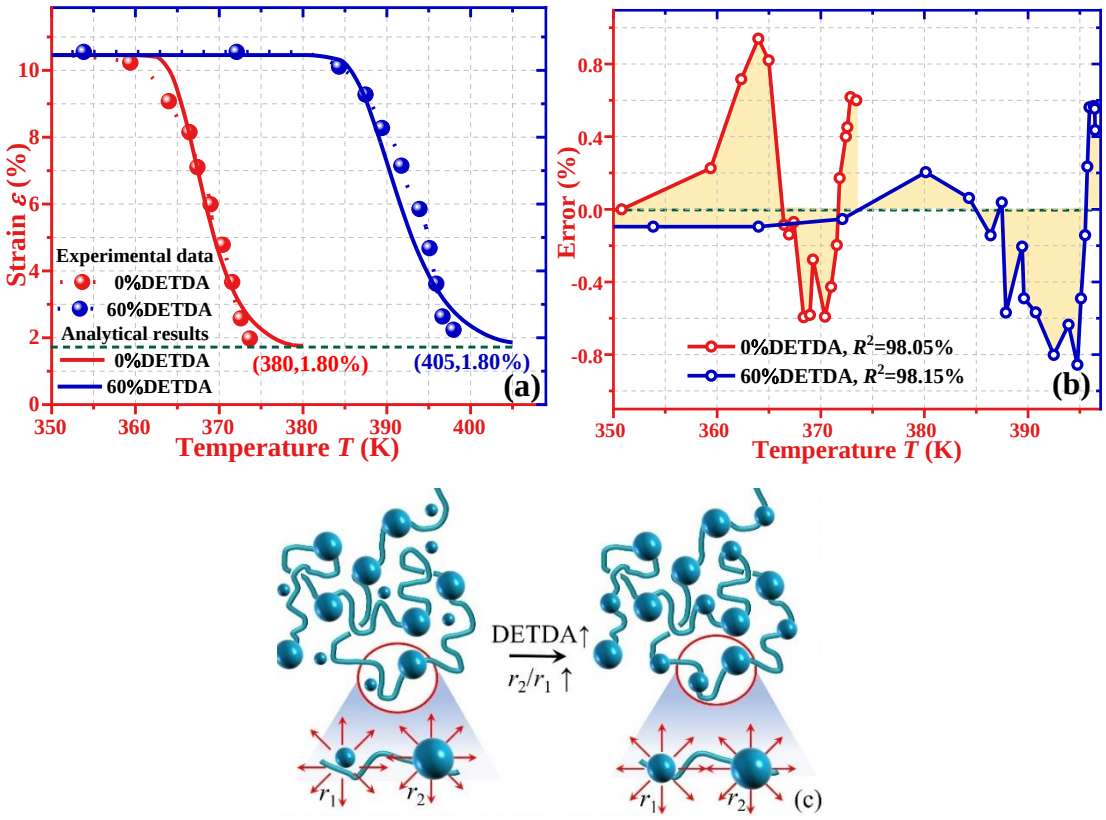

Figure 7. Comparisons of analytical results using equation (10) and experimental data [34] of the strain as a function of temperature for DETDA-D230. (a) The strain-temperature curves. (b) Divergences of analytical and experimental results of strain. (c) Schematic illustration of the effect of DETDA on the radius ratio (r_2/r_1) of CRRs.

Figure 8(a) further plots the analytical results of storage modulus-temperature and experimentally obtained ones for epoxy/amine SMPs with different fractions of Diels-Alder of 0, 0.2, 0.4 and 0.6 [35]. All the parameters used in the calculations based on

equation (12) are listed in Table 3, where τ_0=0.1 s, r_1=1×10^{-9} m, T^{ref}=300 K, T^*=750 K, T_0=265K, G=3 GPa [32,40]. With an increase in the molar ratio of Diels-Alder from 0, 20%, 40% to 60%, the storage modulus is gradually decreased from 21.9 MPa, 7.0 MPa, 4.9 MPa to 3.2 MPa, at the same shape recovery temperature of T=425 K. These analytical and experimental results reveal that the thermomechanical storage modulus of epoxy/amine SMP is essentially determined by the fraction of Diels-Alder agent, which was previously used to decrease the crosslinking density of the polymer network and storage modulus of the epoxy/amine SMP [35]. Figure 8(b) shows the correlation index R^2 between the analytical and experimental results [35], which are 95.47%, 99.35%, 95.76% and 97.92% for the Diels-Alder molar ratios 0, 0.2, 0.4 and 0.6, respectively. Clearly, the analytical results obtained using equation (12) agree well with the experimental data, with their error ratios limited to ±0.6.

Table 3. Values of parameters used in equation (12) for epoxy/amine SMP [35].

Samples	E_{eq} (MPa)	E_{neq} (MPa)	r_2/r_1	α_s (m/K)	α(K^{-1})
0DA	5	1011	0.63	7.49×10^{-12}	0.042
0.2DA		897	1.48	3.10×10^{-11}	0.058
0.4DA		865	4.72	5.11×10^{-11}	0.100
0.6DA		803	16.13	2.98×10^{-11}	0.096

Figure 8(c) illustrates the effect of Diels-Alder on the different radius ratios (r_2/r_1) of the CRRs. It is found that the radius ratio (r_2/r_1) of the CRRs is increased with the increased molar ratio of Diels-Alder, resulting in an increased activation volume (ΔV) of total CRRs and shape recovery temperature of the epoxy/amine SMPs. The working principle of molar ratio of Diels-Alder in the epoxy/amine SMP is attributed to the effect of radius ratio (r_2/r_1) on the activation volume (ΔV) of total CRRs. The

repulsion force has been identified as the driving force [29], and the radius ratio (r_2/r_1) is gradually increased with the increased repulsion force during shoving of the CRR. Therefore, the activation volume (ΔV) is increased, resulting in the decreased repulsion force until a new dynamic equilibrium of storage modulus is reached.

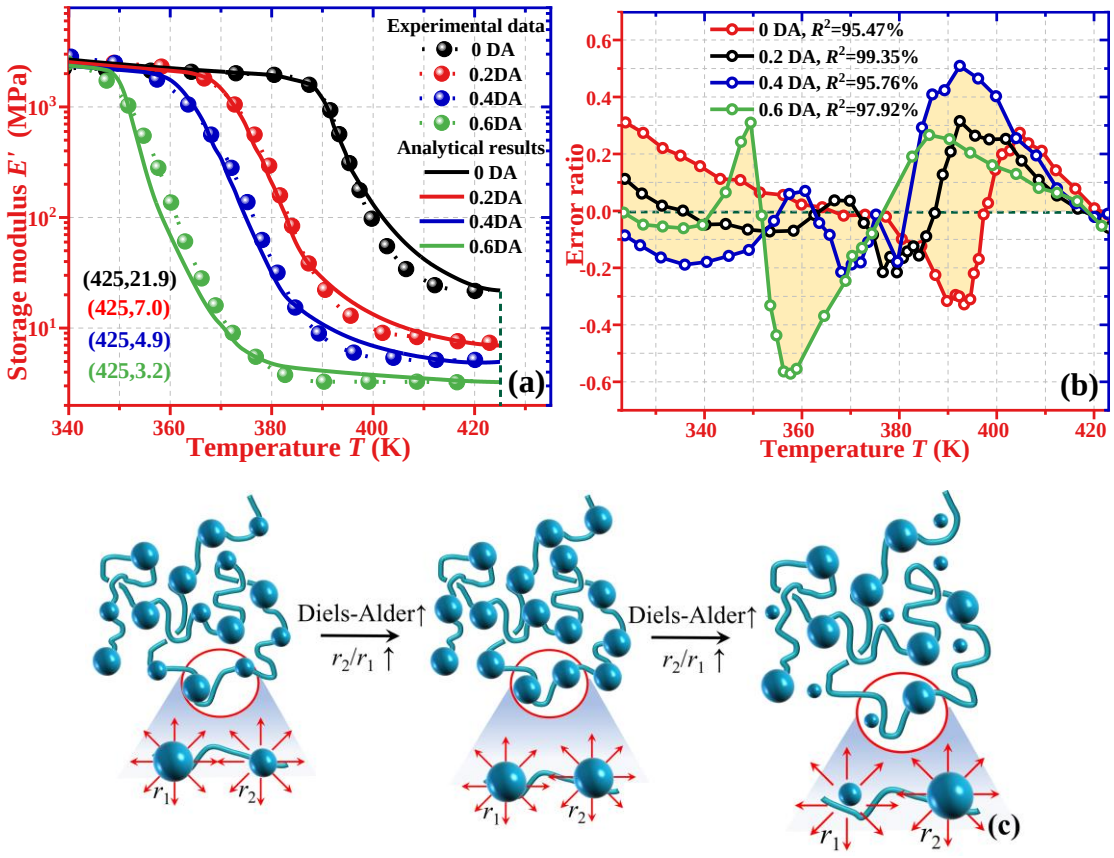

Figure 8. Comparisons of analytical results using equation (12) and experimental data [35] of the storage modulus as a function of temperature for epoxy/amine SMP with different fraction of crosslinking Diels-Alder agent. (a) The storage modulus-temperature curves. (b) Divergences of analytical and experimental results of storage modulus. (c) Schematic illustration of the effect of Diels-Alder on the radius ratio (r_2/r_1) of CRRs.

Finally, the experimental data of DGEBF (DGEBF: diglycidyl ether of bisphenol F) epoxy SMP at various temperatures of 383 K, 393 K, 403 K and 413 K [36] were also been used to compare with the analytical results of stress-relaxation time obtained from equation (14). All the parameters used in the calculation using equation (14) are

listed in Table 4, where τ_0=0.1 s, r_1=1×10^{-9} m, T^{ref}=300 K, T^*=750 K, T_0=265K, G=3 GPa [32,40]. The experimental results and the obtained analytical results are plotted in Figure 9. Results clearly show that with an increase in the shape recovery temperature from 383 K, 393 K, 403 K to 413 K, the relaxation time is gradually decreased from 32 s, 31 s, 30 s to 20 s at the same stress of $(\sigma-\varepsilon_0 E_{eq})/\sigma_0$=e^{-1}, as shown in Figure 9(a). The correlation index R^2 between the analytical and experimental results are obtained as 99.11%, 99.30%, 97.58% and 96.90% for the epoxy at 383 K, 393 K, 403 K and 413 K, respectively, as shown in Figure 9(b).

Table 4. Values of parameters used in equation (14) for DGEBF SMP [36].

Temperature	$\varepsilon_0 E_{eq}/\sigma_0$	r_2/r_1	α_s (m/K)	α(K^{-1})
383 K	0.342	2.12	9.26×10^{-12}	0.032
393 K	0.197		9.25×10^{-12}	0.036
403 K	0.182		9.23×10^{-12}	0.042
413 K	0.154		9.19×10^{-12}	0.050

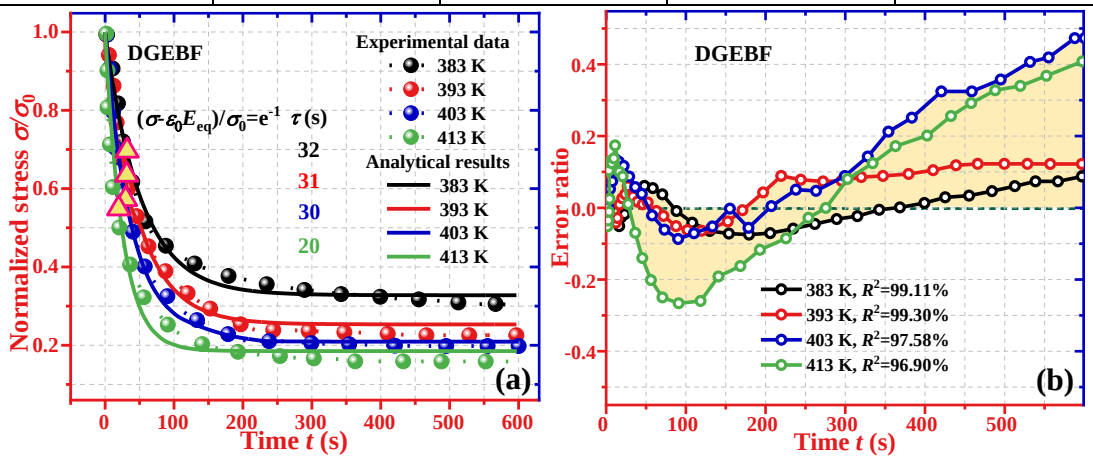

Figure 9. Comparisons of analytical results using equation (14) and experimental data [36] of the stress-relaxation time for DGEBF epoxy SMP at different temperatures. (a) The stress-relaxation time curves. (b) Divergences of analytical and experimental results of normalized stress.

4. Conclusion

In this study, the working principles of glass transition in the amorphous SMPs

(whose thermodynamic SME is mainly governed by the phase transition theory) has been explored using the shoving model. The dynamic fluctuations of potential energy and CRR volume have been identified as the main driving forces for the phase transition and thermodynamic SME in the amorphous SMP. Furthermore, the constitutive stress-strain relationship has been formulated to describe the thermomechanical and shape recovery behaviors of the amorphous SMPs, based on the phase transition theory and extended Maxwell model. Finally, effectiveness of analytical result of proposed model has been verified using the experimental results reported in the literature, and good agreements between these analytical and experimental results of amorphous SMPs are achieved. This study aims on modeling the dynamic fluctuation and its equilibrium to extend the phase transition theory for glass transition, which plays fundamental role to determine the thermodynamic SME and shape recovery behavior in amorphous SMP. Based on our new model, the thermodynamic SME can not only be predictable, but also be designable and tailorable by controlling phase transition.

Data accessibility. Code and data are available at https://github.com/LiuJingyun1019/proceeding-A

Authors' contributions. J.Y.: conceptualization, investigation, methodology, writing—original draft and writing—review and editing; H.L.: conceptualization, funding acquisition, investigation, methodology, writing—original draft and writing—review and editing; Y.Q.: writing—original draft and writing—review and editing.

All authors gave final approval for publication and agreed to be held accountable

for the work performed therein.

Conflict of interest declaration. We have no competing interests.

Funding. This study was financially supported by the National Natural Science Foundation of China under Grant No. 12172107.

References

[1] Herath M, Epaarachchi J, Islam M, et al. Light activated shape memory polymers and composites: a review. Eur Polym J, 2020, 136: 109912

[2] Liu J Y, Lu H B, Fu Y Q. Spinodal dynamics of metastable glass transition domains in amorphous polymer towards thermomechanically tailorable shape memory effect. Sci. China Technol. Sci, doi. 10.1007/s11431-022-2263-7

[3] Xiao R, Huang W M. Heating/solvent responsive shape-memory polymers for implant biomedical devices in minimally invasive surgery: current status and challenge. Macromol Biosci, 2020, 20: 2000108

[4] Buffington S L, Paul J E, Ali M, et al. Henderson J H Enzymatically triggered shape memory polymers. Acta Biomater, 2018, 84: 88–97

[5] Liu J Y, Lu H B, Fu Y Q. Yielding mechanisms for mechano-chemo-thermal couplings in amorphous shape memory polymer undergoing molecular entanglement. J Phys D Appl Phys, 2021, 54: 415302

[6] Lu H B, Liu Y J, Leng J S, et al. Qualitative separation of the effect of the solubility parameter on the recovery behavior of shape-memory polymer Smart Mater Struct, 2009, 18: 085003

[7] Ji S B, Fan F Q, Sun C X, et al. Visible light-induced plasticity of shape memory polymers. ACS Appl Mater Inter, 2017, 9: 3169–3175

[8] Wang X D. A coupling model for the cooperative actuation mechanism of thermochemically responsive shape memory polymers. Smart Mater Struct, 2022, 31: 125001

[9] Wang X D, Jian W, Lu H B, et al. Selective entanglement coupling of nanoparticles in polymer nanocomposite with high shape recovery stress. Compos Sci Technol, 2021, 207: 108728

[10] Meng Q H, Hu J L. A review of shape memory polymer composites and blends Composites: Part A, 2009, 40: 1661–1672

[11] Chen H M, Wang L, Zhou S B. Recent progress in shape memory polymers for biomedical applications. Chinese J Polym Sci, 2018, 36: 905–917

[12] Lendlein A, Langer R. Biodegradable, elastic shape-memory polymers for potential biomedical applications. Science, 2002, 296: 1673–1676

[13] Shi S, Wang J Y, Wang T R, et al. Influence of residual chirality on the conformation and enzymatic degradation of glycopolypeptide based biomaterials. Sci China Tech Sci, 2021, 64: 641–650

[14] Bai Y T, Wang T R, Zhang S L, et al. Recent advances in organic and polymeric carriers for local tumor chemo-immunotherapy. Sci China Tech Sci, 2022, 65: 1011–1028

[15] Zhang Y F, Zhang N B, Hingorani H, et al. Fast-response, stiffness-tunable soft actuator by hybrid multimaterial 3D printing. Adv Funct Mater, 2019, 29: 1806698

[16] Shi M Y, Jiang L J, Yu C J, et al. A robust polyacrylic acid/chitosan cryogel for rapid hemostasis. Sci China Tech Sci, 2022, 65: 1029–1042

[17] Wang S, Brigham J C. A computational framework for the optimal design of morphing processes in locally activated smart material structures. Smart Mater Struct, 2012, 21: 105016

[18] Santo L, Quadrini F, Squeo E A, et al. Behavior of shape memory epoxy foams in microgravity: experimental results of STS-134 mission. Microgravity Sci Technol, 2012, 24: 287–296

[19] Wang Q L, Zhu L, Wei D D, et al. Near-infrared responsive shape memory hydrogels with programmable and complex shape-morphing. Sci China Tech Sci, 2021, 64: 1752–1764

[20] Cohen M H, Turnbull D. Molecular transport in liquids and glasses. J Chem Phys, 1959, 31: 1164–1169

[21] Schweizer K S, Saltzman E J. Theory of dynamic barriers, activated hopping, and the glass transition in polymer melts. J Chem Phys, 2004, 121: 1984–2000

[22] Liu J Y, Gorbacheva G, Lu H B, et al. Dynamic equilibria with glass transition heterogeneity and tailorable mechanics in amorphous shape memory polymers. Smart Mater Struct, 2022, 31: 075022

[23] Liu J Y, Xing Z Y, Lu H B, et al. Interfacial confinement in semi-crystalline shape memory polymer towards sequentially dynamic relaxations. Int J Appl Mech, 2021, 13: 2150117

[24] Nguyen T D, Yakacki C M, Brahmbhatt P D, et al. Modeling the relaxation mechanisms of amorphous shape memory polymers. Adv Mater, 2010, 22: 3411–3423

[25] Liu Y P, Gall K, Dunn M L, et al. Thermomechanics of shape memory polymers: uniaxial experiments and constitutive modeling. Int J Plasticity, 2006, 22: 279–313

[26] Li Y X, He Y H, Liu Z S. A viscoelastic constitutive model for shape memory polymers based on multiplicative decompositions of the deformation gradient. Int J Plasticity, 2017, 91: 300–317

[27] Li Y X, Hu J Y, Liu Z S. A constitutive model of shape memory polymers based on glass transition and the concept of frozen strain release rate. Int J Solids Struct, 2017, 124: 252–263

[28] Wang X D, Jian W, Lu H B, et al. Modeling strategy for enhanced recovery strength and a tailorable shape transition behavior in shape memory copolymers. Macromolecules, 2019, 52: 6045–6054

[29] Dyre J C, Olsen N B, Christensen T. Local elastic expansion model for viscous-

flow activation energies of glass-forming molecular liquids. Phys Rev B, 1996, 53: 2171–2174

[30] Lappala A, Zaccone A, Terentjev E M. Polymer glass transition occurs at the marginal rigidity point with connectivity z(star)=4. Soft matter, 2016, 12: 7330–7337

[31] Adam G, Gibbs J H. On the temperature dependence of cooperative relaxation properties in glass-forming liquids. J Chem Phys, 1965, 43: 139–146

[32] Treloar L R G. The physics of rubber elasticity. Oxford University Press, Oxford, 2005

[33] Xu W M, Pan Y, Deng J N, et al. Reprocessable and self-healing shape memory epoxy resin based on biphenyl mesogen and siloxane. Macromol Chem Phys, 2021, 222: 2100290

[34] Liu H C, Li J B, Gao X X, et al. Double network epoxies with simultaneous high mechanical property and shape memory performance. J Polym Res, 2018, 25: 24

[35] Lorero I, Rodriguez A, Campo M, et al. Thermally remendable, weldable, and recyclable epoxy network crosslinked with reversible Diels-alder bonds. Polymer, 2022, 259: 125334

[36] Liu H C, Zhang H, Wang H, et al. Weldable, malleable and programmable epoxy vitrimers with high mechanical properties and water insensitivity. Chem Eng J, 2019, 368: 61–70

[37] Stevenson J D, Schmalian J, Wolynes P G. The shapes of cooperatively rearranging regions in glass-forming liquids. Nat Phys, 2006, 2: 268–74

[38] Richeton J, Schlatter G, Vecchio K S, et al. A unified model for stiffness modulus of amorphous polymers across transition temperatures and strain rates. Polymer, 2005, 46: 8194–8201

[39] Matsuoka S, Quan X. Intermolecular cooperativity in dielectric and viscoelastic relaxation. J Non-Cryst Solids, 1991, 131: 293–301

[40] Liu J Y, Gorbacheva G, Lu H B, et al. A dynamic hysteresis model for customized glass transition in amorphous polymer towards multiple shape memory effects. Smart Mater Struct, 2022, 31: 125022